ORIGINAL PAPER

Climate cyclicity-controlled recurrent bottom-water ventilation events in the aftermath of the Toarcian Oceanic Anoxic Event: the Jenkyns Event

Lorenz Schwark[1,2] · Wolfgang Ruebsam[1]

Abstract

Environmental perturbations of the Toarcian Anoxic Event and its associated carbon isotope excursion (CIE) occurred in a cyclic fashion indicating an orbital control mechanism. Sedimentary strata of the *E. elegantulum* ammonite subzone in the Lorraine Sub-basin, Luxembourg, exhibit eight sedimentary cycles, most of which postdate the CIE, implying that its termination did not coincide with a full recovery from environmental stress. Sea-level and temperature fluctuations of the Toarcian crisis were linked to a cryosphere demise in the Northern Hemisphere, which modulated stadial versus interstadial phases on the orbital 100 ka eccentricity frequency band. Upon stadial phases, enhanced wind strength in combination with lowered sea level disrupted stratified shelf waters and shifted the storm wave base close to the sea floor. Ventilation of bottom waters interrupted accumulation of laminated and organic-rich black shales, but formed organic-lean and non-laminated gray claystones enriched in terrigenous wax lipids and spores provided via aeolian transport from the hinterland due to the enhanced wind strength. Wind systems are assumed to have been driven by high pressure differences between the cryosphere in the North of the Tethyan shelf and the warmer costal lowland. This distinguishes the atmospheric turbulences after the CIE from the postulated intensification of the cyclones that accompanied the rapid warming at the beginning of the CIE. The deep-water ventilation event following the CIE in the Lorraine Sub-basin was accompanied by a parallel evolution in the SW German Basin, indicating a supraregional driving mechanism in paleobathymetric sub-basins susceptible to lowering of storm wave base. In sub-basins with greater water depth on the NW-Tethyan shelf, post-CIE orbitally driven atmospheric turbulences had a minor or no effect on water column stratification and deposition of organic-rich laminated black shales persisted.

Keywords Orbitally forced black shale formation · Cyclic deposition · Freshwater stratification · Wind strength · Hydrological cycle · Lorraine Sub-basin

Introduction

The climate of the lower Jurassic for long times has been considered to have been of equable and warm conditions (Frakes et al. 1992). The past two decades though provided ample evidence that the Pliensbachian was substantially cooler than the Toarcian and that both climate states were not equable, but showed substantial climate oscillations (Suan et al. 2010; Korte and Hesselbo 2011; Dera and Donnadieu 2012; Krencker et al. 2019; Gómez et al. 2016; Ruebsam et al. 2019; Ruebsam and Schwark 2021; Nordt et al. 2022; Merkel and Munnecke 2023). In the Northwest Tethyan Shelf (NWTS), the magnitude of temperature oscillations was in the range of 10 °C between the outgoing Pliensbachian (22 °C) and the maximum of the so-called Toarcian Anoxic Event (T-OAE). Here, sea surface temperatures of up to 32 °C prevailed as determined by molecular paleothermometry using the TEX$^H_{86}$-ratio (Ruebsam et al. 2020a). For the T-OAE in the Lorraine Sub-basin (Fig. 1.) an orbitally forced cyclic depositional regime in the 100 ka eccentricity frequency band has been documented (Ruebsam et al. 2014, 2019, 2022a). Cyclicity
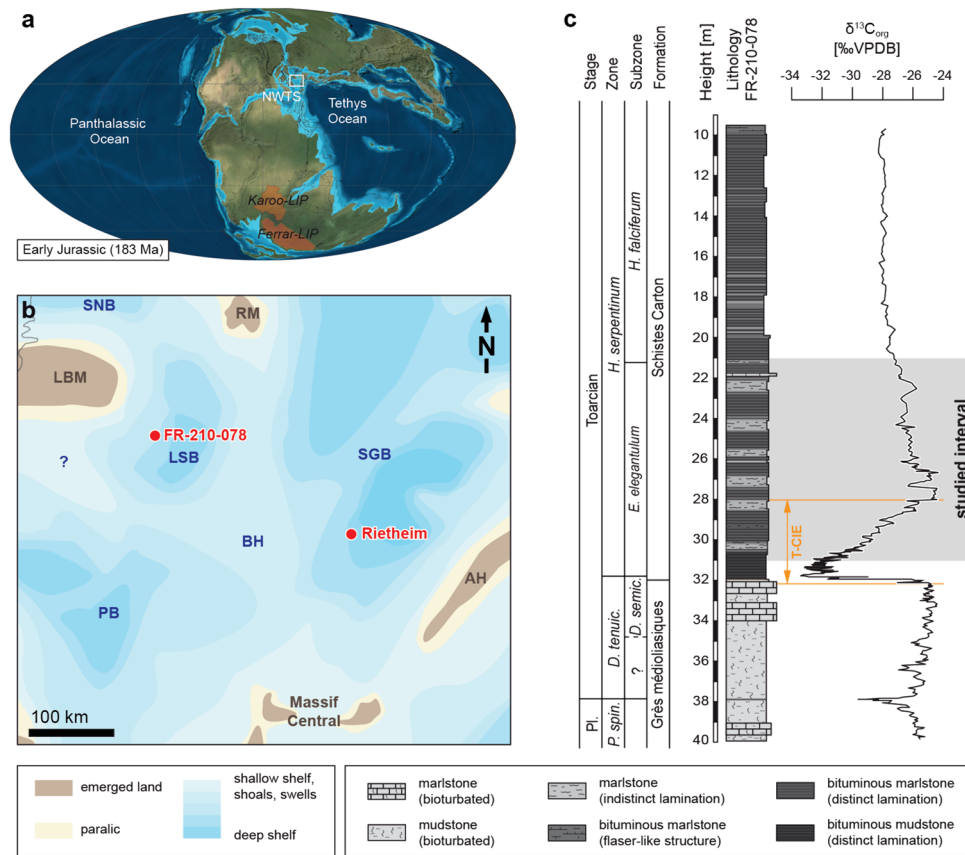
Fig. 1 a Global paleogeographic reconstruction after Blakey (2016) illustrating the region investigated as part of the Northwest-Tethys Shelf (NWTS). **b** Paleogeographic reconstruction of the Paris Basin and adjacent areas (modified from Enay et al. 1980; Mégnien 1981; Mascle 1994; Thierry 2000; Röhl et al. 2001). The study site (Core FR-210–078) is located in the Lorrain Sub-basin (LSB), a depression extending to the Northeast of the Paris Basin (PB). The Lorrain Sub-Basin and the Paris Basin were separated by submarine shoals and swells. Toward the East, the Lorrain Sub-basin borders the South German Basin (SGB). Additional abbreviations: AH: Ale-

mannic High; BH: Burgundy High; LBM: London-Brabant Massif; RM: Rhenish Massif; SNB: South-Netherland Basin). **c** Lithology, biostratigraphy and carbon isotope (δ13C) chemostratigraphy of Core FR-210–078 (from Ruebsam et al. 2014, 2019). The Toarcian Carbon Isotope Excursion (T-CIE) marks the condensed base of the Schistes Carton Formation (*tenuic.: tenuicostatum*; *spin.: spinatum;* Pl.: Pliensbachian). In Core FR-210–078, the central part of the Schistes Carton Formation (gray interval, middle-upper *E. elegantulum* subzone, 21–31 m) shows a profound lithological variability that is a subject of this study

is lithologically expressed by intercalations of gray claystones into the typical Toarcian black shales.

Within the T-OAE that is characterized by the widespread occurrence of black shales deposited under anoxic/euxinic conditions in the wake of a global sea-level rise (Jenkyns and Clayton 1986; Jenkyns 1988, 2010; Littke et al. 1991a, 1991b; Farrimond et al. 1988, 1989; Röhl et al. 2001; Ruebsam et al. 2019, 2020b), a profound Toarcian Carbon Isotope Excursion (T-CIE) has been recognized and attributed to a global environmental perturbation, the Jenkyns Event, which released vast amounts of isotopically depleted carbon into the atmosphere, whereby the carbon source and release mode is still under debate (e.g., Sælen et al. 1996; Hesselbo et al. 2000, 2007; Schouten et al. 2000; Röhl et al. 2001; Kemp et al. 2005; Ruebsam et al. 2014, 2019; Xu et al. 2018; Fantasia et al. 2018).

The environmental perturbations of the Jenkyns Event in the Lorraine Sub-basin extend further into the stratigraphic record than the well-established T-CIE (Ruebsam et al. 2019). This indicates that the end of the latter did not mark a full return to conditions as prevailing prior to the T-CIE. We here investigate whether the environmental perturbations in the *E. elegantulum* ammonite subzone occur on a rhythmic scale and whether a potential cyclicity is governed by orbital driving factors. If orbitally controlled cyclic sedimentation styles do prevail in the *E. elegantulum* subzonal strata of the Lorraine Sub-basin, we further investigate how climate changes affected sediment and organic matter supply to the basin and preservation within the sediment. To analyze sediment type and fabric, water column salinity, stratification and oxygenation, sediment and organic matter supply from the continent by eolian or riverine transportation, and

to develop a conceptual model of alternating climate states, we employ a multidisciplinary approach, employing sedimentology, organic petrology, major and trace element geochemistry, carbonate isotope geochemistry and molecular organic geochemistry.

Study site

This study is based on investigations carried out on an exceptionally well-preserved sediment core (FR-210–078) drilled in southern Luxembourg. During the Early Jurassic, the study site was situated in a northeastern extension of the Paris Basin (Lorraine Sub-basin), a local depression in the shallow marine northwestern West Tethys Shelf (Fig. 1b). The core comprises upper Pliensbachian and lower Toarcian strata, attributed to the Grés médioliasiques Formation and the Schistes Carton Formation. Biozones have been defined by occurrences of age-diagnostic ammonites (Guérin-Franiatte et al. 2010). High-resolution $\delta^{13}C_{org}$ chemostratigraphy provides additional stratigraphic guidance (Fig. 1c) and confirmed that Core FR-210–078 represents a valuable sediment archive recording early Toarcian environmental changes (Ruebsam et al. 2014, 2019, 2022a, 2022b). The cyclicity observed for the study interval has been documented previously (Ruebsam et al. 2014, 2019) and is illustrated in the supplement (Figs. S1, S2).

The base of the Schistes Carton Formation (upmost *D. semicelatum* Subzone–lower *E. elegantulum* subzone) that hosts the onset and core of the early Toarcian Carbon Isotope Excursion (T-CIE) is strongly condensed (Ruebsam et al. 2014, 2019). It follows an interval 31–21 m (most of the *E. elegantulum* subzone) that shows a remarkable lithological variability (Fig. 1c).

Methodology

Continuous non-destructive XRF-core scanning was performed on the un-sampled core-half to guide in the selection of discrete samples subjected to geochemical analysis. Individual samples were crushed and powdered to obtain homogeneous and representative study material. Prior to analyses, samples were dried in an oven at 40 °C for 48 h to remove residual moisture.

X-ray fluorescence core scanning

X-ray fluorescence (XRF)-core scanning was performed using an Itrax XRF core scanner (Cox Analytical Systems, Sweden). The core scanner uses an Si-drift detector (SDD) in combination with a multi-channel analyzer (MCA), which allows counting rates up to 70 kcps with only a minor

degradation in resolution. The device was equipped with a Cr tube that was set to 30 kV and 30 mA, sufficient to detect light elements (Al–Fe). XRF scanning was performed at a resolution of 1 cm with an integration time of 20 s per measurement.

Elemental analysis (ICP-OES)

Major and minor trace elements contents were determined via ICP-OES analysis (inductively coupled plasma-atomic emission spectroscopy) performed by Activation Laboratories Ltd. (Canada). Powdered samples were first digested with aqua regia, a partial digestion that uses a mixture of hydrochloric and nitric acid to dissolve sulfides. Oxides and silicates are only partially dissolved. Therefore, 0.5 g of powdered sample material was digested with aqua regia for 2 h at 95 °C. Afterward, the samples were cooled down and diluted with deionized water. Dissolved elements were analyzed via ICP-OES using a Varian Vista 735 ICP-OES. The accuracy and reproducibility of the analysis were monitored by running replicate analysis of laboratory standards and duplicate analysis of samples.

Organic and inorganic carbon analysis

The total organic carbon (TOC) content was determined on decalcified samples using a Vario CNS Elemental Analyzer EL III (Elementar®). Decalcification was achieved by treating samples with HCl (10% and 25%) to remove calcium carbonate and dolomite. Subsequently, the samples were washed and neutralized with deionized water and dried in an oven at 40 °C for 48 h. Values determined on decalcified samples were corrected for their carbonate loss to yield original TOC concentrations. The reproducibility and accuracy were checked by running replicate analysis of laboratory standards and by duplicate analysis of samples and were better than 0.1 wt% (1σ). The calcite-equivalent carbonate content was calculated by multiplying the inorganic carbon content (TIC) by 8.33 (stoichiometry of $CaCO_3$). TIC was determined by subtracting TOC from the total carbon content (TC), the latter obtained from analyzing the original samples via a Vario CNS Elemental Analyzer EL III (Elementar®).

Rock–Eval pyrolysis

Organic matter was characterized by Rock–Eval pyrolysis using a Rock–Eval II analyzer (Vinci Technologies®) according to the method described by Espitalié et al. (1977). The amount of hydrocarbons generated from the kerogen is expressed as hydrogen index (HI) calculated from the S2 (mgHC/gTOC) values using the formula: $HI = (S2 \times 100)/TOC$. The amount of CO_2 released from pyrolysis of organic

matter (mgCO$_2$/gTOC) is expressed as oxygen index (OI) and calculated as OI = (S3 × 100)/TOC. The temperature of maximum release of pyrolyzate is recorded as Tmax (°C). Reproducibility and accuracy were checked by running replicate analysis of laboratory standards and by duplicate analysis of samples.

Molecular geochemistry

Molecular geochemical analysis was carried out for selected samples following the procedures described in Ruebsam et al. (2022a, b). Briefly, samples were solvent extracted with dichloromethane/methanol (9:1; v/v), followed by compound class fractionation via SPE into aliphatic hydrocarbons, aromatic hydrocarbons and polar fractions by elution with hexane, hexane/dichoromethane (3:1; v/v) and methanol. The aliphatic hydrocarbon fraction was analyzed for biomarker compositions using GC/MS.

Organic petrography

Whole-rock samples were cut from the core and polished block sections were prepared following the international standard procedure ISO7404–2: (2009) (E). Petrographic analyses were performed by Walter Pickel at the Coal & Organic Petrology Services Pty Ltd.. Microscopic photographs were taken using a Keyence digital microscope VHX-700F.

Results and discussion

Lithological and geochemical variations

Visual inspection of Core FR-210–078 revealed the recurrent intercalation of eight grayish and non-laminated intervals of up to 80 cm thickness within the typical laminated black shales of the *E. elegantulum* subzone of the lower Toarcian succession (Ruebsam et al. 2014). The grayish intercalations exhibit an orbitally linked rhythmicity in the 100 ka eccentricity frequency band (Figs. S1, S2). Lithological variation indicates severe changes in depositional conditions, arguing against a monotonous black shale facies, only interrupted by carbonate banks or concretion layers as reported from other locations in the NWTS (Jenkyns 1988; Littke et al. 1991a, 1991b; Farrimond et al. 1988, 1989; Röhl et al. 2001; Kemp et al. 2005; Montero-Serrano et al. 2015; Fantasia et al. 2018). High-resolution but non-quantitative XRF-core scanning of carbonates and siliciclastics, the main rock-forming components, demonstrates a systematic lithological and lithochemical cyclicity within the *E. elegantulum* subzonal section (Fig. 2). The sediment`s carbonate fraction complementary determined by quantitative elemental

analysis yielded absolute carbonate concentrations varying from 10 to 80 wt%, with laminated black shales yielding higher and gray intercalations yielding lower carbonate content. The XRF-scanning response to Si in the gray intercalations was substantially higher than for the black shale (Fig. 2) indicative of carbonate dilution of the siliciclastic fraction in the latter. The siliciclastic fraction reveals a differentiation between the gray intercalations and the black shales by enhanced Si/Al ratios in the latter, pointing toward either their higher biogenic silica content or a higher proportion of detrital quartz. The sedimentary textures of gray intercalations exhibit a lack of lamination (Fig. 2 B and C), which in contrast is prominent in the typical black shale facies (Fig. 2A and D). The absence of lamination is indicative of a higher dynamic regime providing oxygen close to the sediment/water interface, and leading to mixing and homogenization of bottom sediments in the Lorraine Subbasin. In addition to the eight visually detected gray intercalations, XRF-scanning data identify an additional event (7a) at 23.5 m depth via low Ca and high Si proportions of the sediment. Intercalation 5 and the subsequent black shale interval both are marked by a reduced thickness, which is attributed to either condensation, or the presence of hiatuses in this part of the section. The presence of a hiatus at a comparable stratigraphic position has been reported from the Sancerre Core in the southern Paris Basin (Thibault et al. 2018) and is also indicated in coeval strata from other areas (e.g., Ruebsam and Al-Husseini 2020; Ruebsam et al. 2020b).

The systematic lithological and geochemical variation within the so-called black shale provides evidence for rhythmic changes in the sedimentary regime. This was controlled by sediment delivery from the hinterland, surface productivity of the carbonate factory, and bottom-water ventilation during intervals of gray claystone deposition, which caused sediment mixing, bioturbation and organic matter degradation.

Organic matter composition and preservation

The rhythmic variation in sediment composition and fabric is accompanied by coeval changes in the composition of organic matter and its state of preservation. Within the typical black shale facies, TOC contents are substantially higher than in gray claystones, in particular, if calculated on a carbonate free base (Fig. 3) to eliminate the effect of carbonate dilution. In addition to differences in the quantity of organic matter, variation in its quality are documented by decreased HI values in the gray claystones, indicative of both a higher degradation of organic matter and/or a higher proportion of allochthonous land plant influx (Bordenave et al. 1993; Peters et al. 2005). Rock–Eval analysis alone does not allow to reliably differentiate between these two processes. The
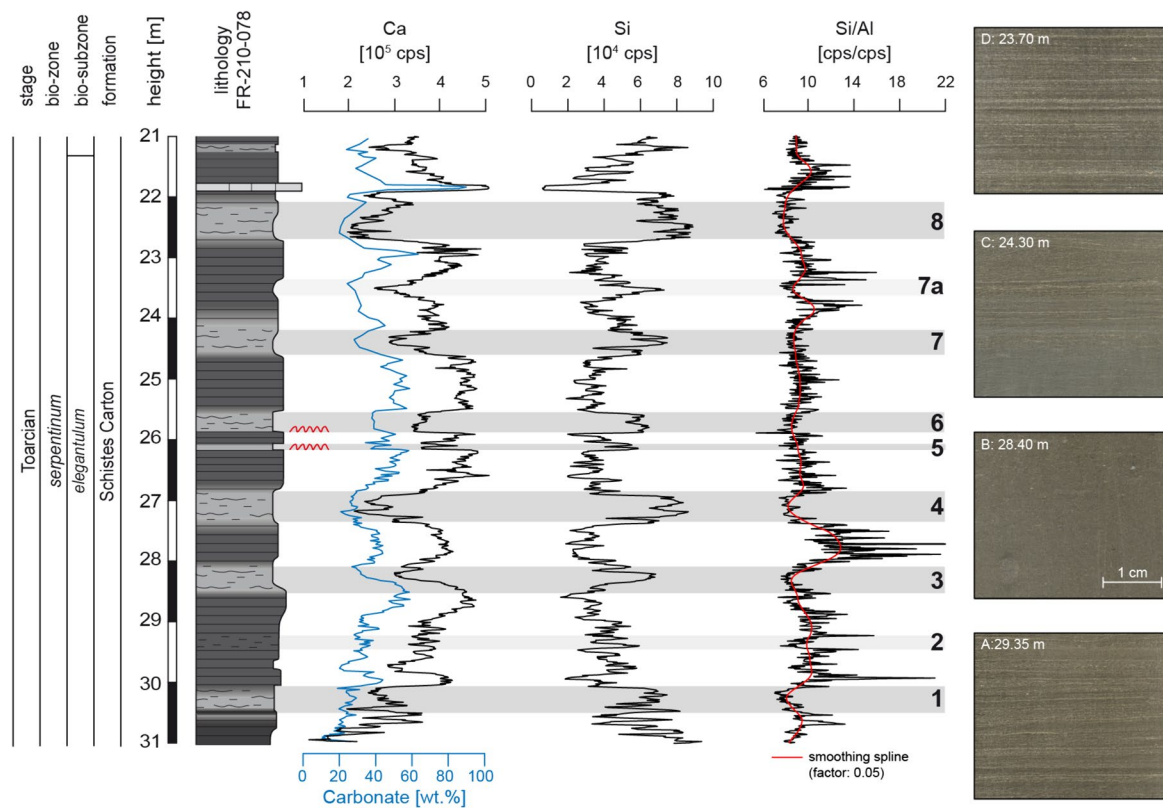
Fig. 2 Lithological and geochemical variation in so-called homogenous black shales of the Toarcian *E. elegantulum* subzone identifies eight lithological cycles of typical laminated black shale and gray homogeneous claystones. XRF-core scanner data reveal the presence of an additional cycle 7a not recognized in visual core inspection. Cycle 5 reveals reduced thickness in both black shale and gray claystone intercalation due to condensation

molecular composition of the extractable bitumen fraction conducted on a subset of samples at reduced stratigraphic resolution allows a more profound recognition of allochthonous land plant influx into the marine Lorraine Sub-basin via epicuticular wax lipids. Hereby, land plant wax *n*-alkanes with longer chain length are contrasted with those of shorter chain length that are derived from marine algae and cyanophytes, as expressed by the terrestrial/aquatic ratio (TAR) established by Bourbonniere and Meyers (1997) and shown in Fig. 3. Gray claystone lithologies exhibit a pronounced increase in TAR values, indicative of an increased delivery and deposition of allochthonous terrigenic material. This information is corroborated by enhanced values of the carbon preference index (CPI) that reflects the relative proportion of *n*-alkanes with an odd number of carbon atoms versus those with an even number (Bray and Evans 1961). Land plant waxes exhibit a strong preference for *n*-alkanes with an odd number of C atoms in the range of nC_{23} to nC_{33}. The CPI decreases with increasing diagenetic transformation of the lipids to approach values of about 1.0, thus eliminating the primary facies information. Toarcian samples exhibit CPI values > 1.0 and are thus unaffected by diagenesis but reveal information on organic matter origin (Peters et al. 2005).

The gray claystone intervals always exhibit an increase in CPI indicative of land plant influx when compared to the adjacent black shales with lower CPI, thus representing a preferentially autochthonous source of algal *n*-alkanes. The transport pathways of land plant waxes may include riverine but also eolian modes, as plant waxes are sufficiently small to be removed from plant needle/leaf surfaces by wind erosion (Simoneit 1977; Simoneit and Mazurek 1982). Higher land plant wax input thus is not a unique criterion for fluvial discharge.

The photosynthetic pigment chlorophyll contains the isoprenoidal lipid phytol as a side chain that is cleaved during diagenesis and transformed into aliphatic isopranes pristane (Pr) and phytane (Ph). These isoprenoids are more susceptible to oxidative degradation of their alcohol functionality than the straight chain *n*-alkane hydrocarbons with 17 or 18 carbon atoms. Isoprenoids are thus preferably removed during oxidative eogenesis (Peters et al. 2005). The ratios of Pr/nC_{17}, Ph/nC_{18} or $(Pr + Ph)/(nC_{17} + nC_{18})$ thus reflect the oxidation potential or oxygen deficiency of the depositional setting, i.e., within the lower water column and the pore water. The gray claystone bands systematically reveal substantially lower $(Pr + Ph)/$
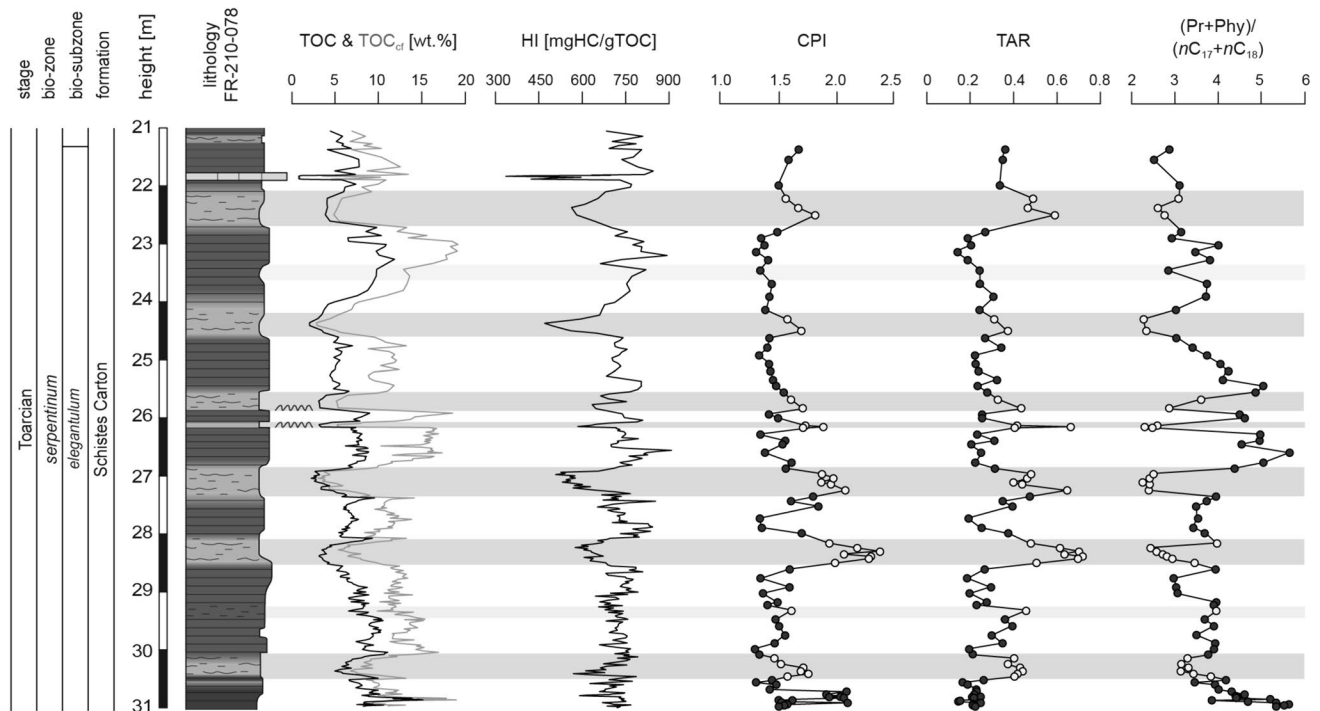
Fig. 3 Stratigraphic variation in quantity, quality and composition of the sedimentary organic matter. Black shale intervals are characterized by increased TOC (and TOC_{cf}) contents and by higher abundances of well-preserved marine organic matter, as indicated by increased HI, lowered TAR, lowered CPI and increased ratios of $(Pr+Phy)/(nC_{17}+nC_{18})$. On the contrary, gray claystones show lowered TOC (and TOC_{cf}) contents, resulting from the enhanced aerobic degradation of labile marine organic matter. Accordingly, gray claystones are characterized by lowered HI, higher TAR, higher CPI and lowered $(Pr+Phy)/(nC_{17}+nC_{18})$ ratios

$(nC_{17}+nC_{18})$ ratios (Fig. 3), which indicates deposition under more oxic conditions within the water column that was established by bottom-water ventilation. The high $(Pr+Ph)/(nC_{17}+nC_{18})$ ratios of the black shales indicate deposition under oxygen-deficient or even euxinic conditions in bottom and pore waters (Frimmel et al. 2004; Peters et al. 2005). These establish under stagnant conditions with water column stratification, a scenario typical for Toarcian black shales (e.g., Wignall 1991; Sælen et al. 1996; Schouten et al. 2000; Schwark and Frimmel 2004; McArthur et al. 2008).

Compositional differences in lipid biomarkers from the black shale lithofacies versus the gray claystone lithofacies for the latter attribute to higher allochthonous organic matter flux into the basin. During deposition of the gray claystones, the water column of the Lorraine sub-basin was not permanently stratified. A third-order sea-level lowstand (Fig. S1) enhanced deep-water ventilation. This state of the paleo-ecosystem differs severely from the autochthonous organic productivity under stratified water columns with anoxic or even euxinic conditions reported from most of the Toarcian strata in the NWTS (e.g., Farrimond et al. 1989, 1994; Littke et al. 1991a, 1991b; Littke 1993; Moldowan et al. 1986; van Kaam-Peters et al. 1998; Schouten et al. 2000; Schwark and Frimmel 2004; French et al. 2014; Song et al. 2017; Ruebsam et al. 2018).

The paleobathymetric/paleogeographic conditions of sediment deposition prevailing during the Toarcian *E. elegantulum* subzone must have made the Lorraine Sub-basin highly sensitive to environmental changes not recorded or not reported to that extent from other regions on the NWTS. This may be attributed to the bowl-shaped bathymetry of the basin (Fig. 1), where the basin center is surrounded by submarine swells, limiting water circulation. Changes in sea level, current strength and direction, depth of wave base and other physiogeographical constraints will thus have been severely modulated by the height of the water column above the surrounding submarine swells.

The compositional and spatial distribution differences in organic matter composition of gray claystones versus black shales on the microscale cannot be addressed by biomarker analysis of solvent-extracted sediment sections that integrate over a few centimeters of the succession. Organic petrology of polished blocks under fluorescent light though reveals the spatial arrangement of particularly the figured organic components, although these represent only a fraction of the total organic matter, most of which is amorphous (Taylor et al. 1998). The photomicrographs of the black shale sample illustrate the abundant occurrence of algal or cyanobacterial mats oriented parallel to bedding and confirm a dominance of marine organic matter (Fig. 4). The photomicrograph of a
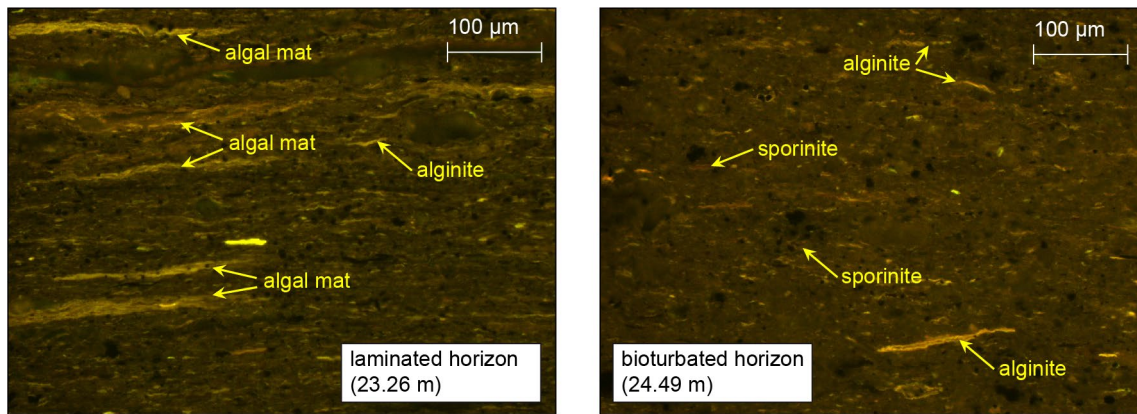
Fig. 4 Representative microphotographs (in incident light fluorescence mode) from polished blocks for two different facies types identified in Core FR-210–078 (laminated black shale versus bioturbated gray claystones). Samples from distinctly laminated horizons contain high concentrations of alginite, which can occur as algal/cyanobacterial mats. Samples from indistinctly laminated and bioturbated horizons show a significantly lower abundance of alginites and are enriched in allochthonous sporinites

gray claystone sample (Fig. 4) demonstrates a general lack of lamination and the absence of intact algal or cyanobacterial mats. These, if originally having been present, were disrupted by hydrodynamic forces mixing the sediment when exposed to wave action or contour currents. In addition to the presence of organoclasts from marine algae, the presence of sporinites indicates elevated aeolian land plant input, which is in accordance with the biomarker composition. The claystone sediments do not exhibit the occurrence of huminites/vitrinites derived from woody plant material and no inertinites or funginites that may originate from terrestrial fungi. This may indicate that the land plant material was preferentially transported by eolian processes but not by fluvial discharge, as this would have carried woody and fungal organoclasts into the Lorraine Sub-basin as well.

The bulk organic geochemical data, the biomarker composition and the organic petrology results demonstrate contrasting sedimentary regimes prevailing between the black shales and the gray claystones due to variable proportions of allochthonous versus autochthonous sediment and biomass input, opposite oxygen deficiency regimes, variable hydrodynamic energy at the sea bottom and thus preservation of organic matter. The effect of environmental conditions between the two contrasting regimes on the marine bioproducer community cannot be fully elucidated with these methods.

To assess shifts in marine organismic composition, triterpenoid biomarkers are employed as indicators for different algal classes and cyanobacteria. A fundamental difference between eukaryotic algae and prokaryotic cyanobacteria results from their cellular membrane composition. Prokaryotes contain hopanoids as cell membrane rigidifiers, whereas in algae steroids serve for this function (Peters et al. 2005). The ratio of steroids versus hopanoids thus enables to allocate the relative proportion of each of the two primary producer groups. The relative proportion of algal steroids is always diminished in the gray claystones (Fig. 5), indicating that upon deposition of these, the algal productivity declined compared to that delivered by cyanophytes. The biological sources of steroids are manifold, including algae, land plants, Animalia and fungi (Peters et al. 2005; Schwark and Empt 2006; Volkman 2016).

A molecular geochemical reconstruction of primary producers in the Lorraine Sub-basin based on steroid and hopanoid triterpenoids, complemented by calcareous nanoplankton investigations, was conducted by Ruebsam et al. (2022b) covering the Toarcian Carbon Isotope Excursion (T-CIE) interval in Core FR210-078 between a core depth of 28–32 m. This represents the core section preceding the interval in the *E. elegantulum* subzone investigated here for bottom-water ventilation events. Biological sourcing of steroids from large Animalia and fungi can be neglected for the marine sediments in the Lorraine Sub-basin, leaving an attribution to zooplankton versus land and aquatic plant origin. Land plants contain steroids preferentially with 29 carbon atoms (Huang and Meinschein 1979; Volkman 2016), but certain algal classes may also be rich in C_{29} steroids (Volkman 2016). Hence, a bifold origin or C_{29} steroids from algae and land plants is feasible, whereby Chlorophyceae (green algae) and Phaeophyceae (brown algae) are considered as the main sources of algal C_{29} steroids (Volkman 2016). The increased contribution of C_{29} steroids in the gray claystones can thus be attributed to both a higher land plant influx as evidenced by the TAR and CPI ratio and an increasing contribution of Chlorophyceae to the algal community. An origin from Phaeophyceae is considered less likely, as these algae started to diversify from the Cretaceous onward (Bringloe et al. 2020). Chlorophycean algal
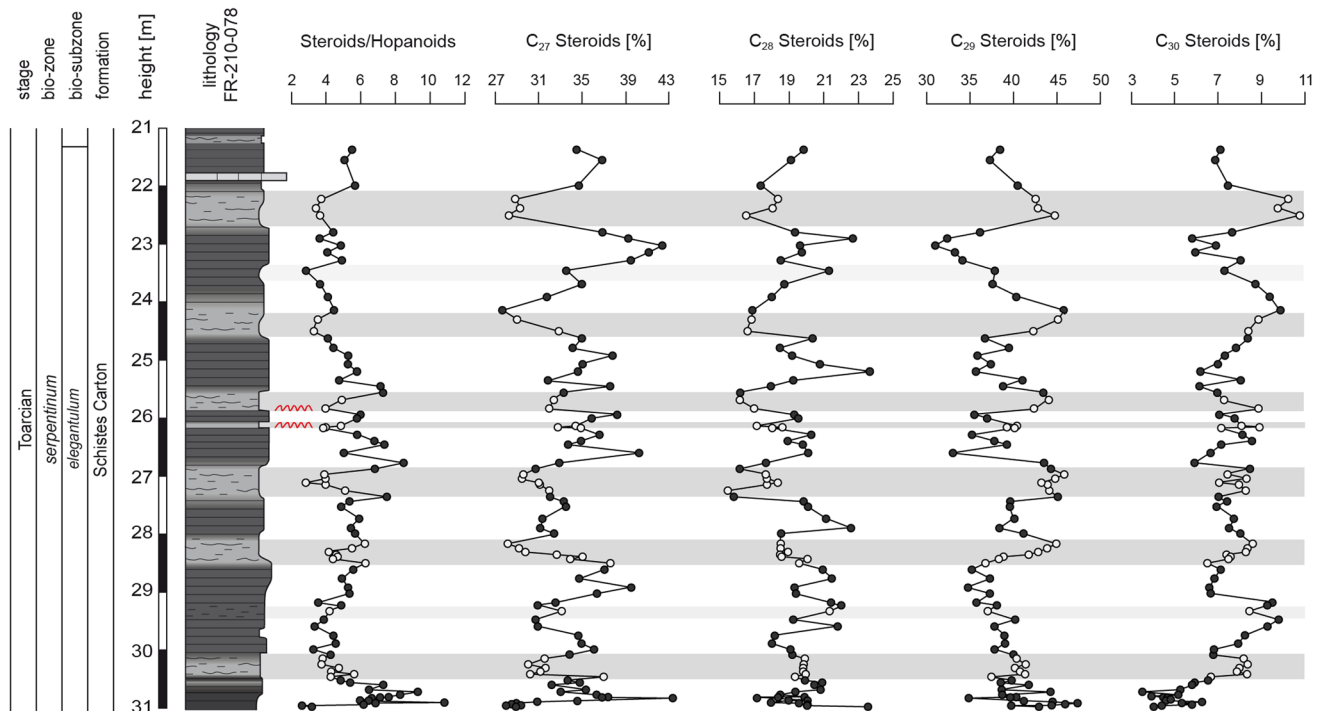
Fig. 5 Triterpenoid biomarker distribution for reconstruction of primary producer and zooplankton associations. A high ratio of steroid/hopanoids may indicate enhanced nutrient supply in freshened surface waters during deposition of black shales. Carbon numbers of steroids suggest variation in terrestrial influx of land plant lipids by elevated %C_{29} upon aeolian transport during gray claystone deposition. Increased continental runoff during warm and humid climates delivered nutrients to sustain coccolithophorid and prasinophyte algal growth, as seen by elevated %C_{28} within black shale horizons. Fully marine conditions with nutrient limitations favored pelagophyte algae as shown by high %C_{30} proportions. High surface productivity sustained zooplankton communities as suggested by elevated %C_{27} steroids

or land plant contributions thus may have increased during deposition of the gray claystones, whereas in contrast, the C_{27} steroids, which are either attributed to a Rhodophyceae or zooplankton origin (Huang and Meinschein 1979; Peters et al. 2005), exhibit a marked decline. This opposite trend in C_{27} vs. C_{29} steroids has also been noted for the deeper section of the core, representing the T-CIE (Ruebsam et al. 2022b), whereby the end of the T-CIE was associated with a marked increase in C_{27} steroid proportions. Low proportions of C_{27} steroids in the gray claystones here are seen as indication of zooplankton breakdown, due to a decline in surface water photosynthetic productivity upon fully marine conditions with nutrient depletion.

Among the algal steroid classes, the regular sterols with 30 carbon atoms and unbranched side chain are exclusively biosynthesized by algae of the pelagophyte, chrysophyte or dinoflagellate type and have not been reported from land plants, fungi or Animalia. The parallel evolution of C_{29} and C_{30} steroids suggests a fully marine and normal salinity environment during deposition of gray claystones. The C_{28} steroids are biosynthesized by a variety of algae including Bacillariphyceae, Haptophyceae and Prasinophyceae (Volkman 2016). As a diatomaceous origin can be ruled out for

the Early Jurassic, an origin from Haptophyceae or Prasinophyceae is assumed. Both algal types have been reported to thrive in Toarcian shelfal waters (Prauss et al. 1991; Prauss 1996; Röhl et al. 2001; Ruebsam et al. 2022b; Mutterlose et al. 2022). Prasinophyceae are highly adapted to oxygen-deficient conditions and hyposalinity of surface waters (Prauss 1996; Schwark and Empt 2006) and thus flourish during deposition of the black shales in severely stratified water bodies. In parallel, coccolithophorid algae will also bloom in nutrient-rich surface waters, contributing to the higher carbonate export production noted for the black shale intervals.

Adaption of primary producers in the Toarcian Lorraine Sub-basin thus indicates fully marine and ventilated conditions during deposition of gray shales, when reduced surface runoff diminished marine productivity and led to a zooplankton decline. Main algal classes were Pelagophytes and Chlorophytes, accompanied by a higher relative abundance of Cyanophytes, potentially adapted to low nutrient availability via diazotrophy. Upon deposition of the black shales, increased freshwater runoff provided high nutrient availability, turned surface waters brackish and favored algal over cyanobacterial growth. Algal communities were dominated

by calcifying haptophytes (coccolithophorids) and green prasinophytes, which supported a food chain with abundant zooplankton species.

Redox regime and bottom-water ventilation events

The redox regime within the lower water body and the pore water during deposition of sediments in the Lorraine Sub-basin fluctuated severely as indicated by various elemental and biomarker proxies (Fig. 6). During times of black shale deposition, the redox regime of the Lorraine Sub-basin in the aftermath of the T-CIE and its upper part was comparable to most parts of the NWTS where stagnant conditions with anoxic to even euxinic bottom waters prevailed (e.g., Schwark and Frimmel 2004; Montero-Serrano et al. 2015). Organic matter accumulation and composition in sediment from Core FR-201–078 in the Lorraine Sub-basin indicate fluctuating environmental conditions, with substantial variation in surface water productivity, which via export flux impacted on oxygen consumption and deficiency in bottom and pore waters. Paleoredox regimes can be reconstructed using diagnostic trace element ratios (Tribovillard et al.

2006; Algeo and Rowe 2012) or molecular biomarker proxies (Peters et al. 2005). Strata of the *E. elegantulum* subzone developed in black shale facies exhibit enrichment of redox-sensitive elements, e.g., vanadium and nickel normalized to aluminum (Fig. 6). In black shale facies, lamination is well preserved (Fig. 2, 4), and the low proportions of iron versus sulfur indicate a preferential fixation in the form of metal sulfides, dominantly pyrite, under reducing to euxinic conditions. Oxygen deficiency during black shale deposition is corroborated by enhanced preservation of labile organic molecules, e.g., via preservation of hopenes with extended side chains (Schwark et al. 1998; Peters et al. 2005;) as shown in Fig. 6. In contrast, gray claystones generally are depleted in extended C_{35}-hopenes.

Reconstruction of paleosalinity and water column stratification

The paleoenvironmental reconstruction discussed above emphasized the role of salinity in shaping the environment, by regulating the marine primary producer community, trophic cascade, organic matter accumulation and
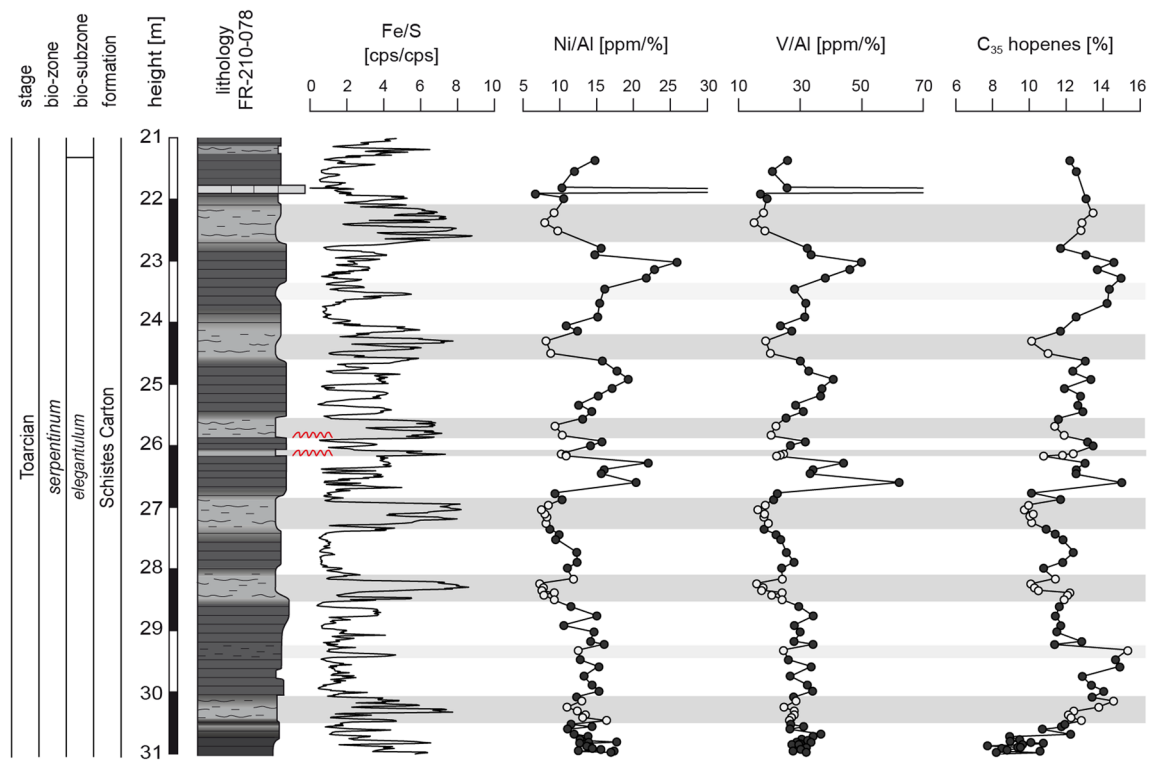

Fig. 6 Trace element and biomarker redox proxies indicate an oxic regime with abundant ferric iron versus sulfur delivered via eolian dust supply into a fully marine and bottom ventilated marine realm during deposition of gray claystones. Upon deposition of black shales, enhanced continental runoff led to freshwater stratification, surface productivity blooms and anoxic to euxinic conditions in bottom and pore waters, where trace elements Ni and V became fixed in sulfides and complexed in organic matter. Oxygen-deficient conditions favored the preservation of the side chain in hopene triterpenoids (C_{35} hopenes %) during deposition of black shales, whereas gray claystones are depleted in extended hopenes

preservation. Surface water freshening in parts of the NWTS have been previously documented based on biological indicators involving prasinophytes or ostracods (Prauss and Riegel 1989; Arias 2013), as well as oxygen isotopic composition of bulk or biogenic carbonate (Sælen et al. 1996; Röhl et al. 2001), inorganic trace element proxies, particularly boron enrichment (Remírez and Algeo 2020) and molecular biomarker indicators, namely the degree of alkylation of methyltrimethyltridecylchromanes, expressed as the MTTC ratio (Ruebsam et al. 2022b).

We here employ the oxygen isotope proxy determined on bulk carbonates and the molecular organic geochemical paleosalinity biomarker, the MTTC proxy. The $\delta^{18}O$ isotope ratio of marine carbonates formed under regular salinity ranges between $-2‰$ and $+2‰$ (VPDB), whereby shifts to lighter isotopic composition indicates fresh water being depleted in the ^{18}O isotope (e.g., Sharp 2017). The MTTC ratio utilizes an empirically established response in alkylation, whereby hyposaline conditions are expressed in a higher degree of alkylation (Sinninghe Damsté et al. 1987; Schwark et al. 1998; Tulipani et al. 2015; Ruebsam et al. 2018, 2022b).

Both the isotopic and molecular geochemical salinity proxies (Fig. 7) indicate a trend to hyposaline conditions prevailing during deposition of black shales and a trend to normal marine salinity upon deposition of gray claystones.

Reduced salinities in surface waters of Toarcian sediments depend on freshwater supply by riverine runoff (Ruebsam et al. 2022b) or a monsoonal climate system (Röhl et al. 2001) with intensive monsoonal rain events. Previous studies discussed the occurrence of permanent hyposalinity for the entire Toarcian Anoxic Event (Sælen et al. 1996; Röhl et al. 2001), without differentiating rhythmic salinity fluctuations. Recent investigations (Ruebsam et al. 2022b) found evidence that salinity fluctuation during the T-CIE may have been controlled by orbital forcing in the 100 ka or short eccentricity orbital frequency band. Salinity fluctuations were initiated by a third-order sea-level fall coinciding with the *E. elegantulum* subzone (Fig. S1; Fig. 7).

Hyposalinity induced by freshwater runoff will not only influence marine bioproducer community structures via organismic salinity tolerance, but also via runoff-associated nutrient supply. The combination of freshwater runoff establishing a freshwater surface layer on top of saline bottom waters with the enhanced nutrient supply supported algal/cyanobacterial blooms, which substantially enhanced the organic matter flux to the seafloor. Oxidation of settling organic matter consumed dissolved oxygen in bottom waters, turning these anoxic, which induced organic matter enrichment in black shales. The periods of diminished freshwater runoff disturbed water column stratification and allowed for bottom water oxygenation, as elaborated above.
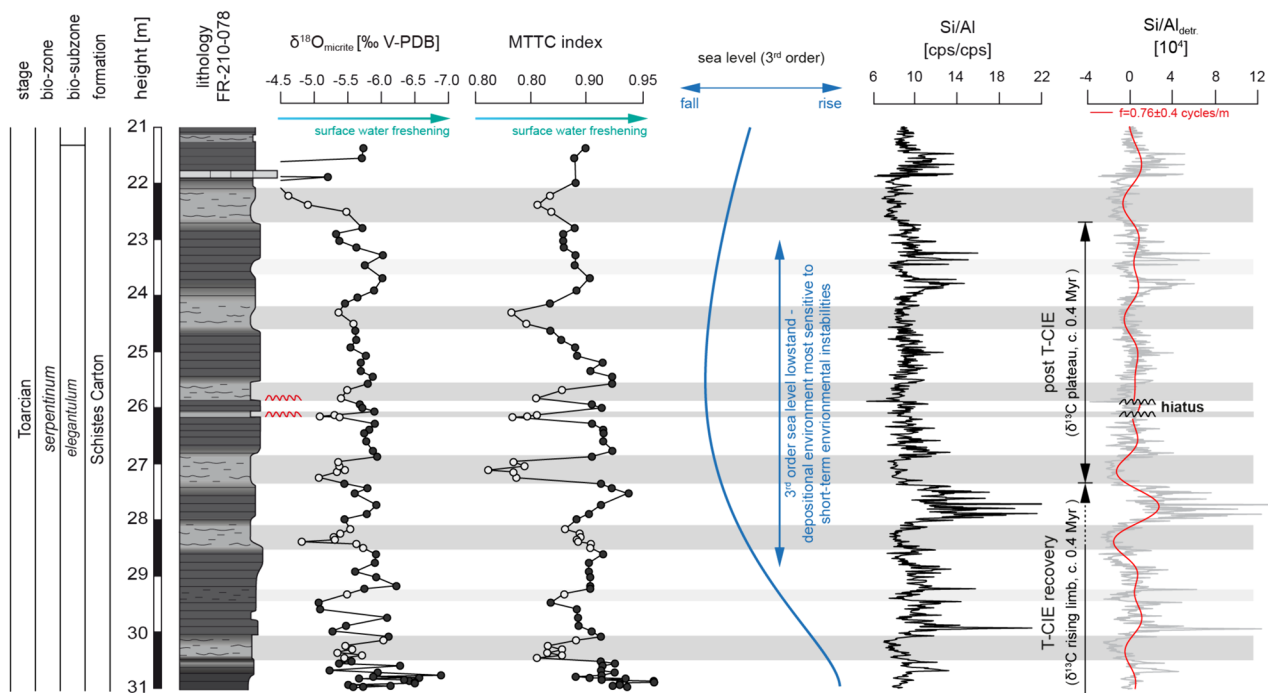

Fig. 7 Fluctuations in paleosalinity as indicated by the $\delta^{18}O$ isotope ratio of micritic carbonate and the molecular paleosalinity proxy based on alkylation of methyltrimethyltridecylchromans (MTTC-index) occurred during a period of third-order sea-level lowstand (Ruebsam et al. 2020a). Enhanced eolian dust flux during gray claystone deposition indicated by diminished Si/Al-ratios occurred in a 100 ka rhythm (Ruebsam et al. 2019; Fig. S2) enforced by orbital eccentricity

Periods of deep-water ventilation and gray shale deposition experienced a higher flux of terrestrial wax lipids (Fig. 3) and spores (Fig. 4) indicative of enhanced wind transport energy that was sufficient to mix shelfal waters down to the sea floor. This enhanced eolian transport capacity would have been fostered by higher wind strength due to a different air pressure regime over the Northern Hemisphere. In contrast to previous climate models (Frakes et al. 1992) postulating an overall warm lower Jurassic, it has been shown that the warm period of the Toarcian was preceded by a colder climate state prevailing through the Pliensbachian (Dera et al. 2011; Korte and Hesselbo 2011; Dera and Donnadieu 2012; Gómez et al. 2016; Ruebsam et al. 2020a; Ruebsam and Schwark 2021; Nordt et al. 2022) that established an extensive cryosphere in the Northern Hemisphere (Ruebsam and Schwark 2021). Not only the Pliensbachian (Korte and Hesselbo 2011; Gómez et al. 2016), but also the Toarcian (Ruebsam et al. 2019) times were subject to multiple climate fluctuation. Waxing and waning of the Northern Hemisphere cryosphere were modulated in the 100 ka short eccentricity orbital frequency band (Ruebsam et al. 2019, 2020b). Formation of the wind strength-driven gray claystone intercalations in the Lorraine Sub-basin follows

a 100 ka cyclicity (Fig. 7; Fig. S2) in the same rhythmicity as during the middle and upper T-CIE interval. The breakdown phase of the cryosphere afforded substantial time including the late T-CIE interval, but must have persisted at least 400 ka longer as evidenced by the occurrence of wind strength-driven deep-water ventilation in the Lorraine Sub-basin (Fig. 7; Fig. S2). We thus hypothesize that a major driver of cyclic sedimentation in the Toarcian Lorraine Sub-basin was climate controlled by periods of enhanced wind strength, driven by extension of the Northern Hemisphere cryosphere as illustrated schematically in Fig. 8. The high-pressure regime over elevated regions in the Northern Hemisphere channeled katabatic winds downward toward the low-pressure shelf regions and its lowland coastal plains enforcing wind strength to a level of deep-water ventilation in the Lorraine Sub-basin. The alternations of gray claystones and black shales in the latest phase and in the aftermath of the T-CIE are thus a combined product of both alternating freshwater stratification and wind-driven deep-water ventilation.

Comparable variation in fluctuations of wind strength and cyclone intensity have been postulated by Krencker et al. (2019) based on field studies in Northern Africa where

Fig. 8 Conceptual model of climate glacial/interglacial states of the climate systems postulated for the *E. elegantulum* subzone of the Lorraine and SW-German Basin. Upon interstadial phases (**a**), ice caps in the Northern Hemisphere retracted, sea level rose and intensified hydrological cycle stimulated freshwater runoff from the continent intensifying nutrient flux, freshwater stratification with deep-water anoxia/euxinia leading to deposition of black shales. A low pressure difference between land and ocean caused weak wind systems thus minimizing plant wax and pollen flux to the shelf. Upon stadial phases (**b**), ice caps in the Northern Hemisphere protracted, sea level fell, and a weakened hydrological cycle with low freshwater runoff and nutrient flux caused deep-water ventilation and deposition of gray claystones. A high pressure difference between land and ocean intensified wind systems transporting plant wax and pollen to the shelf and facilitated deep-water mixing
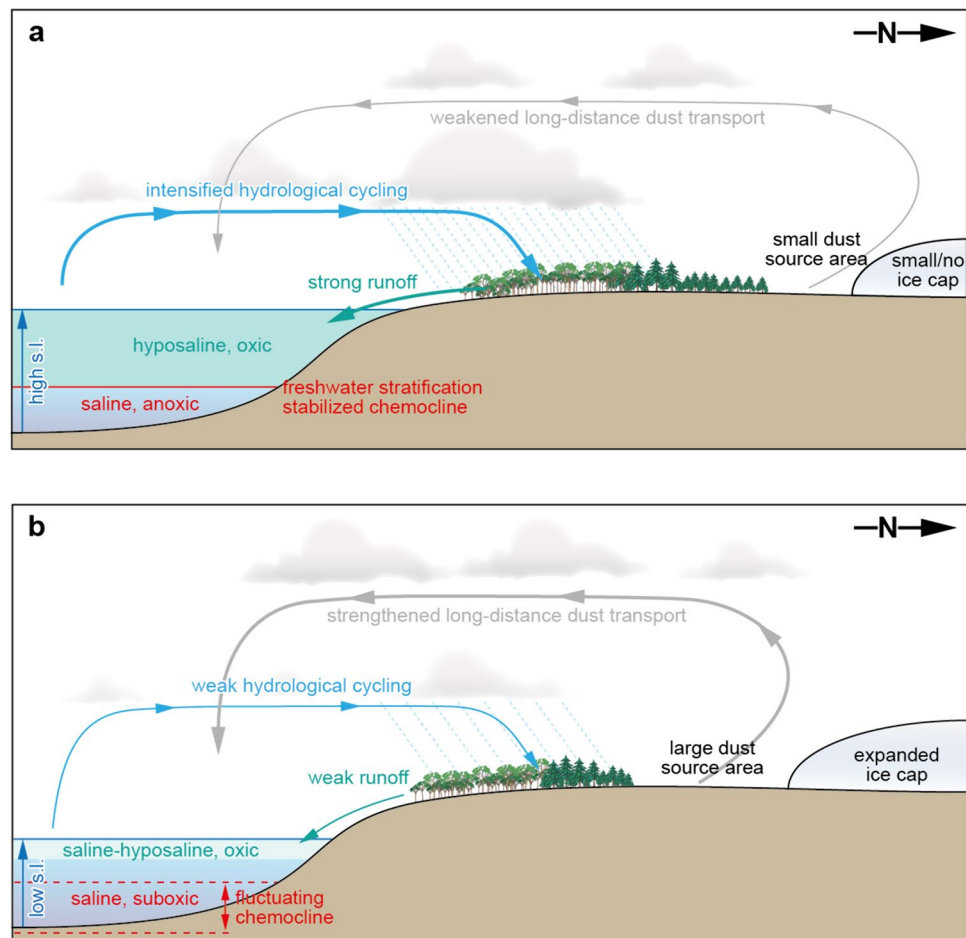
multiple storm deposits and deepening of the storm wave base have been identified in Early Toarcian strata of the High Atlas Basin in Morocco and elsewhere. Yan et al. (2023) based on modeling experiments supported such a cyclone scenario. The storm deposits reported in these studies do not exhibit a cyclicity in the 100 ka frequency band and preferentially occur at the base of the T-CIE rather than during its aftermath, as is the case in the Lorraine Sub-basin. The cyclone-induced storm deposits were supposed to originate from strong cyclones moving from the open Tethys toward the northwestern shelf edge (Krencker et al. 2019) and thus taking a path opposite to the northerly/northeasterly wind system proposed here to have prevailed after the end of the T-CIE. The wind pattern reconstructions by Yan et al. (2023) do show a different wind regime with major wind trajectories in the northwestern Tethys running from the North to the South in the Lorraine region, which is compatible with the wind directions postulated in this study. However, the rhythmic pattern of strong northerly winds as derived here from the interpretation of composition of sediments deposited after the T-CIE seems to be timely decoupled from the cyclones associated with the early Toarcian warming.

Transregional correlation of bottom-water ventilation in the *E. elegantulum* subzone of the NWTS and potential driving forces

The recognition of rhythmic bottom-water ventilation in the Lorraine Sub-basin raises the question whether this is solely a local phenomenon controlled by the physiogeographical constraints of exclusively this sub-basin or if comparable developments can be recognized in other basins as well. If so, this would argue for overarching mechanisms, potentially related to orbital forcing of paleoclimate. Sedimentological features and geochemical profiles at sufficient stratigraphic resolution for sites on the NWTS that cover the *E. elegantulum* subzone post the T-CIE are limited. For the Rietheim core from the SW-German Basin (Fig. 1), a detailed log of TOC (%wt) abundance and the micritic $\delta^{18}O$ isotope ratio is available (Montero-Serrano et al. 2015) that exhibits lithofacies and sedimentary fabric features that mimic the evolution noted in the Lorraine Sub-basin. Although the Rietheim succession exhibits the intercalation of several major carbonate horizons, the eight gray shale intercalations, termed bioturbated horizons in Montero-Serrano et al. (2015) are sedimentogically well defined (Fig. 9). The shallow and restricted shelf depositional environment in the SW-German Basin was comparable with that of the Lorraine Sub-basin and thus expressed a similar sensitivity to wind-driven deepwater ventilation that is not noted in most other sub-basin on the NWTS. Besides the sensitivity of deep-water ventilation, which is controlled by basin bathymetry and windfetch area over the region, the availability of high-quality

and continuous cores may have hindered recognition in other sub-basins featuring comparable bathymetry. In sub-basins, where the water depth was too high, lowering of sea level in combination with enhanced wind strength did not shift the wave base into proximity to the seafloor and thus no bottomwater ventilation and breakup of bottom water anoxia and or euxinia occurred.

In the SW-German and Lorraine Sub-basin, the combination of sea-level drop and wind strength intensification lowered the wave base to the seafloor, thus disrupting the well-known anoxic/euxinic black shale depositional regime by providing deep-water ventilation and associated aerobic degradation of organic matter in non-laminated to bioturbated gray claystones.

Conclusions

Climatic oscillations during the Lower Toarcian occurred on an orbital frequency of 100 ka, equivalent to the short eccentricity that primarily affects climate components in temperate regions, where an insolation-sensitive cryosphere prevailed from the Pliensbachian cold stage into the Lower Toarcian warm phase. Waxing and waning of the temperate cryosphere modulated the strength of high versus low pressure cells and thus the strength of the wind system. Stadial phases led to extensions of ice caps in the Northern Hemisphere, which caused the sea level to fall. Under colder conditions, the hydrological cycle slowed down, thus minimizing freshwater runoff and nutrient flux from the hinterland to the NW Tethyan shelf. A high pressure difference between land and ocean intensified wind systems transporting plant wax and pollen to the shelf. The combination of lower sea level with higher wind strength facilitated deep-water mixing, disrupted algal/bacterial mats and enhanced the supply of oxygen to the seafloor thus enforcing organic matter degradation and bioturbation. Under warm conditions, sea level rose and freshwater and nutrient supply from the continent enhanced, leading to well-stratified water bodies with high productivity and preservation as evidenced by laminated sediments with intact microbial mats and high organic matter content. The two contrasting climate regimes show a preferred eolian sediment, nutrient and organoclast flux for the stadial and a predominantly riverine sediment and nutrient supply with low terrigenous organic matter flux upon the interstadial phases. The stadial/interstadial differences in climate and sedimentation regime are pronounced in basins that due to their bathymetry are susceptible to moderate changes in sea level and wind strength.

Cyclic deposition of gray claystones during stadial intervals postdating the T-CIE seems to decouple the high wind strength events observed for the Lorraine Sub-basin from the intensified cyclone activity previously postulated for the
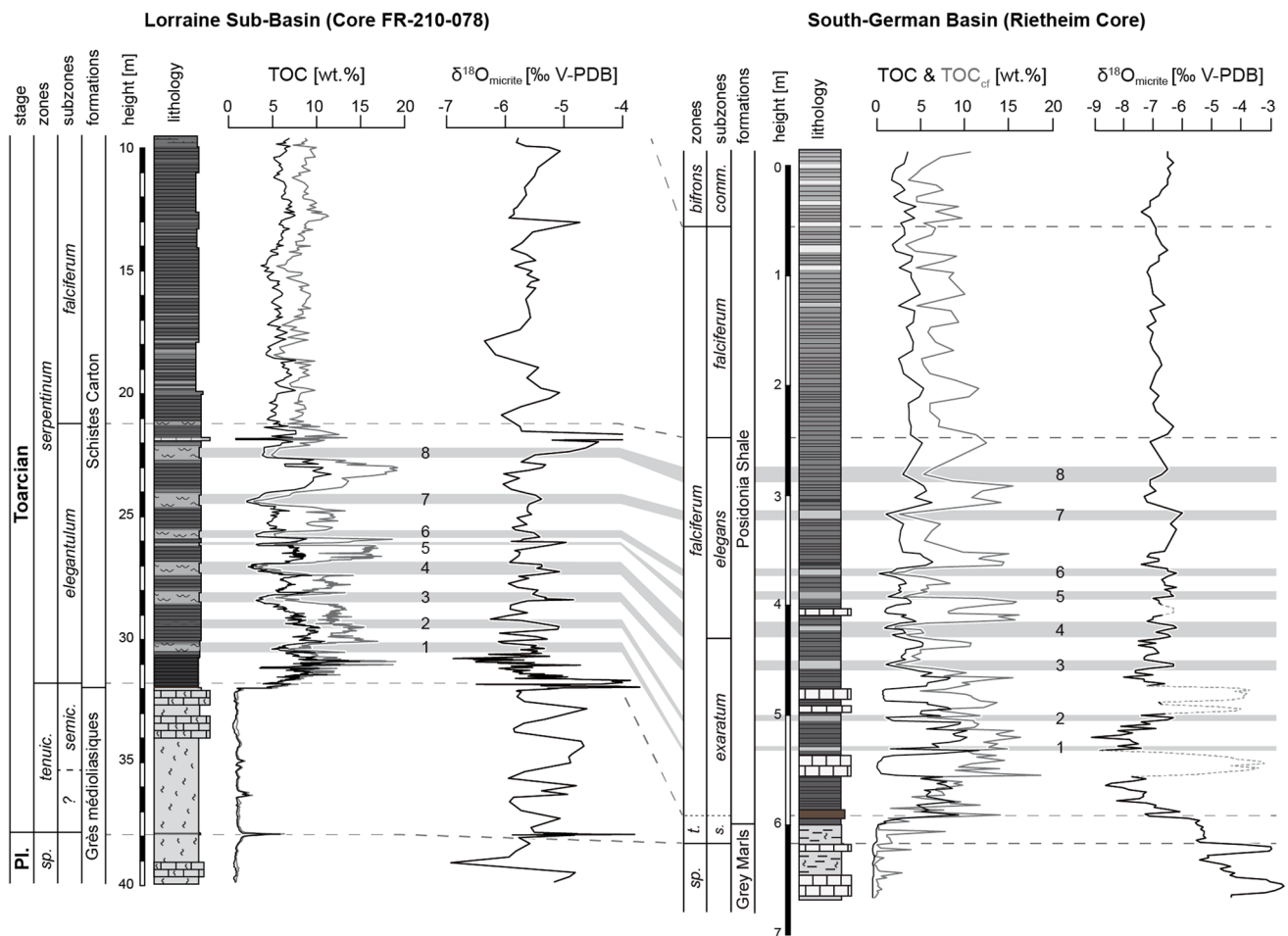
Fig. 9 Correlation of gray claystones indicative of bottom-water ventilation for Core FR-210–078 from the Lorranie Sub-basin with the Rietheim Core (Montero-Serrano et al. 2015) from the SW-German Basin. Correlation is based on TOC values and micrite oxygen isotope proxies available for both locations. The SW-German Basin is affected by a number of carbonate horizons intercalated into the succession, which disturbed the TOC record that has been re-calculated on a carbonate-free base (TOC$_{cf}$). The carbonate intercalations also disrupted the oxygen isotope trend, which has been plotted as a stippled line for the massive carbonate banks. In both cores, eight gray claystones or bioturbated horizons can be parallelized, indicating a supra-regional driving mechanism based on the combined effects of sea-level lowering and enhanced wind strength during stadial periods of the *E. elegantulum* subzone

very early Toarcian warming, which occurred coeval with the onset of the T-CIE.

Declarations

References

Algeo TJ, Rowe H (2012) Paleoceanographic applications of trace-metal concentration data. Chem Geol 324–325:6–18

Arias C (2013) The early Toarcian (early Jurassic) ostracod extinction events in the Iberian Range: The effect of temperature changes and prolonged exposure to low dissolved oxygen concentrations. Palaeogeogr Palaeoclimatol Palaeoecol 387:40–55

Blakey RC (2016) Global Jurassic Paleogeographic Map (180 MaBP): Mollweide. In: Global Paleogeography and Tectonics in Deep Time © 2016. Colorado Plateau Geosystems Inc.

Bordenave ML, Espitalié J, Leplat P, Oudin JL, Vandenbroucke M (1993) Screening techniques for source rock evaluation. In: Bordenave ML (ed) Applied Petroleum Geochemistry. Éditions Technip, Paris, pp 217–278

Bourbonniere RA, Meyers PA (1997) Sedimentary geolipid records of historical changes in the watersheds and productivities of Lakes Ontario and Erie. Limnol Oceanogr 41:352–359. https://doi.org/10.4319/lo.1996.41.2.0352

Bray EE, Evans ED (1961) Distribution of n-paraffins as a clue to recognition of source beds. Geochim Cosmochim Acta 22:2–15

Bringloe TT, Starko S, Wade RM, Vieira C, Kawai H, De Clerck O, Cock JM, Coelho SM, Destombe C, Valero M, Neiva J, Pearson GA, Faugeron S, Serrão EA, Verbruggen H (2020) Phylogeny and evolution of the brown algae. Crit Rev Plant Sci 39(4):281–321. https://doi.org/10.1080/07352689.2020.1787679

Dera G, Brigaud B, Monna F, Laffont R, Pucéat E, Deconinck JF, Pellenard P, Joachimski MM, Durlet C (2011) Climatic ups and downs in a disturbed Jurassic world. Geology 39:215–218. https://doi.org/10.1130/G31579.1

Dera G, Donnadieu Y (2012) Modeling evidences for global warming, Arctic seawater freshening, and sluggish oceanic circulation during the early Toarcian anoxic event. Paleoceanography 27:PA2211. https://doi.org/10.1029/2012PA002283

Enay R, Mangold C, Cariou E, Debrand-Passard S, Donze P, Gabilli J, Lafavrais-Raymond A, Mouterde R, Thierry J (1980) Synthèse paléogéographique du Jurassique français. Villeurbanne. Dép. des sciences de la terre, Université Claude-Bernard, 210 pp.

Espitalié J, Laporte JL, Madec M, Marquis F, Leplat P, Paulet J, Boutefeu A (1977) Rapid method for source rocks characterization and for determination of petroleum potential and degree of evolution. Rev Inst Fr Pétrol 32:23–42

Fantasia A, Föllmi KB, Adatte T, Spangenberg JE, Mattioli E (2018) Expression of the toarcian oceanic anoxic event: new insights from a swiss transect. Sedimentology 66:262–284

Farrimond P, Eglinton G, Brassel SC, Jenkyns HC (1988) The Toarcian black shale event in northern Italy. Org Geochem 13:823–832

Farrimond P, Eglinton G, Brassel SC, Jenkyns HC (1989) Toarcian anoxic event in Europe: an organic geochemical study. Mar Pet Geol 6:136–147

Farrimond P, Stoddart DP, Jenkyns HC (1994) An organic geochemical profile of the Toarcian anoxic event in northern Italy. Chem Geol 111:17–33

Frakes LA, Francis JE, Syktus JI (1992) Climate Modes of the Phanerozoic. Cambridge University Press, Cambridge, UK

French KL, Sepulveda J, Trabucho-Alexandre J, Gröcke DR, Summons RE (2014) Organic geochemistry of the early Toarcian oceanic anoxic event in Hawsker Bottoms, Yorkshire, England. Earth Planet Sci Lett 390:116–127

Frimmel A, Oschmann W, Schwark L (2004) Chemostratigraphy of the Posidonia Black Shale, SW-Germany: I - Influence of Sea Level Variation on Organic Facies Evolution. Chem Geol 206:199–230

Gómez JJ, Comas-Rengifo MJ, Goy A (2016) Palaeoclimatic oscillations in the Pliensbachian (Early Jurassic) of the Asturian Basin (Northern Spain). Climate of the past 12:1199–1214

Guérin-Franiatte S, Maquil R, Münzberger P (2010) Le Toarcian au Grand-Duché de Luxembourg: biostratigraphie dans la region de Belvaux. In: Weis R, Guérin-Franiatte S (Eds.), Le Jurassiques inférieur et moyen au Luxembourg: Nou-velles données paléontologiques et biostratigraphiques. Ferrantia 62: 19–34.

Hesselbo SP, Gröcke DR, Jenkyns C, Bjerrum CJ, Farrimod P, Morgens Bell HS, Green OR (2000) Massive dissociation of gas hydrate during the Jurassic oceanic anoxic event. Nature 406:392–395

Hesselbo SP, Jenkyns HC, Duarte LV, Oliveira LCV (2007) Carbon-isotope record of the early Jurassic (Toarcian) Oceanic Anoxic Event from fossil wood and marine carbonate (Lusitanian Basin, Portugal). Earth Planet Sci Lett 253:455–470

Huang WY, Meinschein WG (1979) Sterols as ecological indicators. Geochim Cosmochim Acta 43:739–745

ISO7404–2: 2009 (E). Methods for the petrographic analysis of coals – part 2: methods of preparing coal samples.

Jenkyns HC (1988) The early Toarcian (Jurassic) Anoxic Event – stratigraphic, sedimentary, and geochemical evidence. Am J Sci 288:101–151

Jenkyns HC (2010) Geochemistry of oceanic anoxic events. Geochem Geophys Geosyst 11:Q03004. https://doi.org/10.1029/2009GC002788

Jenkyns HC, Clayton CJ (1986) Black shales and carbon isotopes in pelagic sediments from the Tethyan Lower Jurassic. Sedimentology 33:87–106

Kemp DB, Coe AL, Cohen AS, Schwark L (2005) Astronomical pacing of methane release in the Early Jurassic period. Nature 437:396–399. https://doi.org/10.1038/nature04037

Korte C, Hesselbo SP (2011) Shallow marine carbon and oxygen isotope and elemental records indicate icehouse-greenhouse cycles during the Early Jurassic. Paleoceanography 26:1–18

Krencker FN, Lindström S, Bodin S (2019) A major sea-level drop briefly precedes the Toarcian oceanic anoxic event: implication for early Jurassic climate and carbon cycle. Sci Rep 9:12518

Littke R, Rotzal H, Leythaeuser D, Baker DR (1991b) Lower Toarcian Posidonia Shale in Southern Germany (Schaebische Alb) Organofacies, depositional environment, and maturity. Erdoel Und Kohle, Erdgas, Petrochemie 44:407–414

Littke R, Baker DR, Leythaeuser D, Rullkötter J (1991a) Keys to the depositional history of the Posidonia Shale (Toarcian) in the Hils Syncline, northern Germany. In: Tyson RV, Pearson TH (Eds.), Modern and Ancient Continental Shelf Anoxia. Geological Society Special Publication 58, pp. 311–333.

Littke R (1993) Deposition, Diagenesis, and Weathering of Organic Matter-rich Sediments. Springer-Verlag, 216 pp

Mascle A (1994) Hydrocarbon and petroleum geology of France. EAPG Special Publications 4, 446 pp.

McArthur JM, Algeo TJ, van de Schootbrugge B, Li Q, Howarth RJ (2008) Basinal restriction, black shales, Re-Os dating, and the early Toarcian (Jurassic) oceanic anoxic event. Paleoceanography 23: PA4217. https://doi.org/10.1029/2008PA001607

Mégnien C (1981) Synthèse géologique du bassin de Paris. Mémoir BRGM n°101, 102, 103.

Merkel A, Munnecke A (2023) Glendonite-bearing concretions from the upper Pliensbachian (Lower Jurassic) of South Germany: indicators for a massive cooling in the European epicontinental sea. Facies 69:10. https://doi.org/10.1007/s10347-023-00667-6

Moldowan JM, Sundararaman P, Schoell M (1986) Sensitivity of biomarker properties to depositional environment and/or source input in the Lower Toarcian of SW-Germany. Org Geochem 10:915–926

Montero-Serrano JC, Föllmi KB, Adatte T, Spangenberg JE, Tribovillard N, Fantasia A, Suan G (2015) Continental weathering and

redox conditions during the early Toarcian Oceanic Anoxic Event in the northwestern Tethys: Insight from the Posidonia Shale section in the Swiss Jura Mountains. Palaeogeogr Palaeoclimatol Palaeoecol 429:83–99

Mutterlose J, Klopschar M, Visentin S (2022) Ecological adaptation of marine floras and faunas across the Early Jurassic Toarcian Oceanic Anoxic Event – A case study from northern Germany. Palaeogeogr Palaeoclimatol Palaeoecol 602:111176

Nordt L, Breecker D, White J (2022) Jurassic greenhouse ice-sheet fluctuations sensitive to atmospheric CO_2 dynamics. Nat Geosci 15:54–59

Peters KE, Walters CC, Moldowan JM (2005) The Biomarker Guide: Volume 2, Biomarkers and Isotopes in Petroleum Systems and Earth. Cambridge University Press, 1132 pp.

Prauss ML (1996) The Lower Toarcian Posidonia Shale of Grimmen, Northeast Germany. Implications from the palynological analysis of a near-shore section. N Jb Geol Paläont 200:107–132

Prauss ML, Riegel W (1989) Evidence from phytoplankton associations for causes of black shale formation in epicontinental seas. N Jb Geol Paläont 11:671–682

Prauss ML, Ligouis B, Luterbacher HP (1991) Organic matter and palynomorphs in the "Posidonienschiefer" (Toarcian, Lower Jurassic) of southern Germany. Geological Society London Special Publications 58:335–351

Remírez MN, Algeo TJ (2020) Paleosalinity determination in ancient epicontinental seas: A case study of the T-OAE in the Cleveland Basin (UK). Earth Sci Rev 201:103072

Röhl HJ, Schmidt-Röhl A (2005) Lower Toarcian (Upper Liassic) black shales of the Central European Epicontinental Basin: a sequence stratigraphic case study from the SW German Posidonia Shale. SEPM Special Publications 82:165–189

Röhl HJ, Schmid-Röhl A, Oschmann W, Frimmel A, Schwark L (2001) The Posidonia Shale (lower Toarcian) of SW-Germany: an oxygen-depleted ecosystem controlled by sea level and palaeoclimate. Palaeogeogr Palaeoclimatol Palaeoecol 165:27–52

Ruebsam W, Al-Husseini M (2020) Calibrating the Early Toarcian (Early Jurassic) with stratigraphic black holes (SBH). Gondwana Res 82:317–336

Ruebsam W, Münzberger P, Schwark L (2014) Chronology of the early Toarcian environmental crisis in the Lorraine Sub-Basin (NE Paris Basin). Earth Planet Sci Lett 404:273–282

Ruebsam W, Müller T, Kovács J, Pálfy J, Schwark L (2018) Environmental response to the early Toarcian carbon cycle and climate perturbations in the northeastern part of the West-Tethys shelf. Gondwana Res 59:144–158

Ruebsam W, Mayer B, Schwark L (2019) Cryosphere carbon dynamics control early Toarcian global warming and sea level evolution. Global Planet Change 172:440–453

Ruebsam W, Reolid M, Sabatino N, Masetti D, Schwark L (2020a) Molecular paleothermometry of early Toarcian climate perturbation. Global Planet Change 195:103351

Ruebsam W, Mattioli E, Schwark L (2022a) Weakening of the biological pump induced by a biocalcification crisis during the early Toarcian oceanic anoxic event. Global Planet Change 217:103954

Ruebsam W, Mattioli E, Schwark L (2022b) Molecular fossils and calcareous nannofossils reveal recurrent phytoplanktonic events in the early Toarcian. Global Planet Change 212:103812

Ruebsam W, Schwark L (2021) Impact of north-hemispherical cryosphere on early Toarcian climate and environmental perturbation. In: Reolid, M., Mattioli, E., Duarte, L.V., Ruebsam, W. (Eds.), Carbon Cycle and Ecosystem Response to the Jenkyns Event in the Early Toarcian (Jurassic). GSL Special Publications 514. https://doi.org/10.1144/SP514-2021-11

Ruebsam W, Thibault N, Al-Husseini M (2020b) Early Toarcian glacio-eustatic unconformities and chemostratigraphic black holes.

In: Montenari, M. (Ed.), Stratigraphy & Timescales, Volume 5, Case Studies in Isotope Stratigraphy, pp. 629–676.

Sælen G, Doyle P, Talbot MR (1996) Stable-isotope analysis of belemnite rosta from the Whitby Mudstone Fm., England: surface water conditions during deposition of a marine black shale. Palaios 11:97–117

Schouten S, van Kaam-Peters HME, Rijpstra WIC, Schoell M, Sinninghe Damsté JS (2000) Effects of an Oceanic Anoxic Event on the stable carbon isotopic composition of early Toarcian carbon. Am J Sci 300:1–22

Schwark L, Empt P (2006) Sterane biomarkers as indicators of palaeozoic algal evolution and extinction events. Palaeogeogr Palaeoclimatol Palaeoecol 240:225–236

Schwark L, Frimmel A (2004) Chemostratigraphy of the Posidonia Black Shale, SWGermany: II. Assessment of extent and persistence of photic-zone anoxia using aryl isoprenoid distributions. Chem Geol 206:231–248

Schwark L, Vliex M, Schaeffer P (1998) Geochemical characterization of Malm Zeta laminated carbonates from the Franconian Alb, SW-Germany (II). Org Geochem 29:1921–1952

Sharp, Z (2017) Principles of Stable Isotope Geochemistry. 2nd Edition. https://doi.org/10.25844/h9q1-0p82

Simoneit BRT (1977) Organic matter in aeolian dusts over the Atlantic Ocean. Mar Chem 5:443–464

Simoneit BRT, Mazurek MA (1982) Organic matter of the troposphere—II. Natural background of biogenic lipid matter in aerosols over the rural western United States. Atmos Environ 16:2139–2159

Sinninghe Damsté JS, Kock-Van Dalen AC, De Leeuw JW, Schenck PA, Guoying S, Brassell SC (1987) The identification of mono-, di- and trimethyl 2 methyl 2 (4,8,12 trimethyltridecyl)chromans and their occurrence in the geosphere. Geochim Cosmochim Acta 51:2393–2400

Song J, Littke R, Weniger P (2017) Organic geochemistry of the Lower Toarcian Posidonia Shale in NW Europe. Org Geochem 106:76–92

Suan G, Mattioli E, Pittet B, Lécuyer C, Suchéras-Marx B, Duarte LV, Philippe M, Regiani L, Francois M (2010) Secular environmental precursors to Early Toarcian (Jurassic) extreme climate changes. Earth Planet Sci Lett 290:448–458. https://doi.org/10.1016/j.epsl.2009.12.047

Taylor GH, Teichmüller M, Davies A, Diessel CFK, Littke R, Robert P (1998) Organic Petrology - A new handbook incorporating some revised parts of Stach's Textbook of Coal Petrology. Borntraeger Publishing, Berlin, p 704

Thibault N, Ruhl M, Ullmann CV, Korte C, Kemp DB, Gröcke DR, Hesselbo SP (2018) The wider context of the Lower Jurassic Toarcian oceanic anoxic event in Yorkshire coastal outcrops. UK Proc Geol Assoc 129:372–391. https://doi.org/10.1016/j.pgeola.2017.10.007

Thierry J (2000) Middle Toarcian. In: Dercourt J, Geatini M, Vrielynck B, Barrier E, Biju-Duval B, Brunet MF, Cadet JP, Crasquin S, Sandulescu M (Eds.), Atlas Peri-tethys, Paleogeographical Maps. Map. 8, pp. 61–70.

Tribovillard N, Algeo TJ, Lyons T, Riboulleau A (2006) Trace metals as paleoredox and paleoproductivity proxies: an update. Chem Geol 232:12–32

Tulipani S, Grice K, Greenwood PF, Schwark L, Böttcher ME, Summons RE, Foster CB (2015) Molecular proxies as indicators of freshwater incursion-driven salinity stratification. Chem Geol 409:61–68

Van Kaam-Peters HME, Schouten S, Köster J, Sinninghe Damsté JS (1998) Controls on the molecular and carbon isotopic composition of organic matter deposited in a Kimmeridgian euxinic shelf sea:

evidence for preservation of carbohydrates through sulfurisation. Geochim Cosmochim Acta 62:3259–3283

Volkman JK (2016) Sterols in microalgae. In: Beardall J, Raven J, Borowitzka MA (eds) Microalgal Physiology. Springer, pp 485–506

Wignall PB (1991) A model for transgressive black shales. Geology 19:167–170

Xu W, Ruhl M, Jenkyns HC, Leng MJ, Huggett JM, Minisini and nine others (2018) Evolution of the Toarcian (Early Jurassic) carbon-cycle and global climatic controls on local sedimentary processes (Cardigan Bay Basin, UK). Earth Planet Sci Lett 484:396–411

Yan Q, Li X, Kemp DB, Guo J, Zhang Z, Hu Y (2023) Elevated atmospheric CO_2 drove an increase in tropical cyclone intensity during the early Toarcian hyperthermal. Proceedings of the National Academy of Sciences: 120 https://doi.org/10.1073/pnas.2301018120